

Mutational signatures in esophageal adenocarcinoma reveal etiologically distinct subgroups with therapeutic relevance

Maria Secrier^{1,*}, Xiaodun Li^{2,*}, Nadeera de Silva², Matthew D. Eldridge¹, Gianmarco Contino², Jan Bornschein², Shona MacRae², Nicola Grehan², Maria O'Donovan², Ahmad Miremadi³, Tsun-Po Yang², Lawrence Bower¹, Hamza Chettouh², Jason Crawte², Nuria Galeano-Dalmau², Anna Grabowska⁴, John Saunders⁵, Tim Underwood⁶, Nicola Waddell^{7,8}, Andrew P. Barbour^{9,10}, Barbara Nutzinger², Achilleas Achilleos¹, Paul A. W. Edwards¹¹, Andy G. Lynch¹, Simon Tavaré¹, Rebecca C. Fitzgerald^{2,‡}, on behalf of the oEsophageal Cancer Clinical and Molecular Stratification (OCCAMS) Consortium[‡]

¹ Cancer Research UK Cambridge Institute, University of Cambridge, Cambridge, UK

² Medical Research Council Cancer Unit, Hutchison/Medical Research Council Research Centre, University of Cambridge, Cambridge, UK

³ Department of Histopathology, Addenbrooke's Hospital, Cambridge, UK

⁴ Queen's Medical Centre, University of Nottingham, Nottingham, UK

⁵ Nottingham University Hospitals NHS Trust, Nottingham, UK

⁶ Faculty of Medicine, University of Southampton, Southampton General Hospital, Southampton, UK

⁷ Department of Genetics and Computational Biology, QIMR Berghofer, Herston, Queensland, Australia

⁸ Queensland Centre for Medical Genomics, Institute for Molecular Bioscience, The University of Queensland, Queensland, Australia

⁹ Surgical Oncology Group, School of Medicine, The University of Queensland, Translational Research Institute at the Princess Alexandra Hospital, Woolloongabba, Brisbane, Queensland, Australia

¹⁰ Department of Surgery, School of Medicine, The University of Queensland, Princess Alexandra Hospital, Woolloongabba, Brisbane, Queensland, Australia

¹¹ Department of Pathology, University of Cambridge, Cambridge, UK

* These authors contributed equally.

‡ Corresponding author.

‡ A full list is available at the end of the manuscript.

Abstract. Esophageal adenocarcinoma (EAC) has a poor outcome, and targeted therapy trials have thus far been disappointing due to a lack of robust stratification methods. Whole-genome sequencing (WGS) analysis of 129 cases demonstrates that this is a heterogeneous cancer dominated by copy number alterations with frequent large scale rearrangements. Co-amplification of receptor tyrosine kinases (RTKs) and/or downstream mitogenic activation is almost ubiquitous; thus tailored combination RTKi therapy might be required, as we demonstrate *in vitro*. However, mutational signatures reveal three distinct molecular subtypes with potential therapeutic relevance, which we verify in an independent cohort (n=87): i) enriched for BRCA signature with prevalent defects in the homologous recombination pathway; ii) dominant T>G mutational pattern associated with a high mutational load and neoantigen burden; iii) C>A/T mutational pattern with evidence of an aging imprint. These subtypes could be ascertained using a clinically applicable sequencing strategy (low coverage) as a basis for therapy selection.

Esophageal cancer is the eighth most common cancer world-wide, and the sixth most common cause of cancer-related deaths [1]. There are two main subtypes, squamous and adenocarcinoma, and the incidence of EAC has increased 4.6-fold amongst white males in the US over the past three decades [2]. It is an aggressive disease, with early loco-regional spread, resulting in a median overall survival of less than a year [3].

Curative treatment has been based on esophagectomy, with the addition of peri-operative chemotherapy or chemoradiotherapy improving survival [4-6]. The use of

molecularly targeted agents has lagged behind that of other cancers and the results so far have been disappointing. Indeed, only Trastuzumab treatment has led to any improvement in outcomes, and this was only in HER2 positive cases, in metastatic disease [7]. Advances in this area have been hampered by the lack of understanding of the molecular drivers of this cancer.

Major sequencing efforts have enabled new classifications of cancers based on their molecular parameters [8, 9]. The emerging genomic biomarkers are based on single nucleotide mutations, structural rearrangements and mutational signatures [10-14], and in some instances these have started to lead to the development of stratified trials with the promise of improved outcomes for patients [15].

Exome sequencing and a small number of whole-genome sequences have uncovered a limited number of potential driver mutations in EAC. However, as many of the mutations occur in tumor suppressor genes (TP53, SMAD4, ARID1A), actionable oncogenic mutations have remained elusive [16, 17]. What is emerging is a picture of genomic instability with complex rearrangements leading to significant heterogeneity between patients [18]. What is still lacking is an understanding of how to use these complex molecular data to stratify patients to help inform clinical decision making.

Here, we present WGS data for over 100 cases performed as part of the International Cancer Genome Consortium, with verification of key findings in independent cohorts. We have used genomic information coupled with expression data and *in vitro* experiments to better understand the failure of targeted therapies and to uncover mechanisms of disease pathogenesis that may inform tumor classification and therapy selection.

RESULTS

Large-scale alterations dominate the EAC landscape

WGS data from 129 EAC patients (including tumors from the gastroesophageal junction, Siewert type 1 and 2) have allowed us to comprehensively catalog the genomic alterations in this cancer, including the large-scale structural rearrangements not detectable from exome sequencing. The clinical characteristics of the cohort are typical for the disease (Supplementary Table 1).

As previously noted, point mutations are abundant in this cancer [16]. However, the overall genomic landscape suggests a disease driven by structural variation and copy number changes (Fig. 1 and Supplementary Fig. 1). Analysis of a combined cohort of 111 EAC cases from TCGA [19] and Nones et al [20] confirms a dominance of copy number alterations, compared to point mutations, in the majority of cases (Supplementary Fig. 2).

When examining the specific loci affected, potential gene driver events were highly heterogeneous between cases, and structural changes again dominated (Fig. 1). For example, when considering genes altered in 10% or more of cases, many more were rearranged, amplified or deleted than were affected by indels or nonsynonymous point mutations. We observed novel recurrently rearranged genes, including SMYD3 in 39% of cases, RUNX1 27%, CTNNA3 22%, RBFOX1 21%, the CDKN2A/2B locus 18%, CDK14 16%, JUP 12% (important transcriptional, signalling and cell communication regulators), and fragile sites (FHIT 95%, WWOX 84%, MACROD2 64%). Somatic L1 mobile element insertions were also abundant. Detecting inserts that had transduced unique flanking

sequences identified an average of 25 inserts/tumor (range 0 to 1127), including those already known to transduce [21, 22] and novel examples. These numbers are substantially higher than previously reported [21] because of improved sensitivity. Mobile element insertions were found in signalling, cell cycle and cell adhesion regulators: ERBB4 - 6/129, CTNNA3 - 5/129, CTNNA2 - 4/129, CDH18 - 3/129, SOX5 - 2/129, CDK12 - 1/129.

Significantly amplified loci according to GISTIC2.0 [23] (7q22, 13q14, 18q11, 11q13 etc.) comprised genes like ERBB2, EFGR, RB1, GATA4/6, CCND1, MDM2 among others, while the top significantly deleted loci in the cohort (9p21, 21p11, 3p14, etc.) showed losses of e.g. CLDN22, CDKN2A, CKN2B, as well as several fragile sites (Supplementary Fig. 3 and Supplementary Tables 2 and 3).

The most frequent somatic mutation/indel events included a number of known driver genes with roles in DNA damage, signal transduction, cell cycle and chromatin remodelling. Seven of these reached statistical significance as likely driver genes, as inferred by MutSigCV [24] (Fig. 1e and Supplementary Table 4): TP53 (81%), ARID1A (17%), SMAD4 (16%), CDKN2A (15%), KCNQ3 (12%), CCDC102B (9%), CYP7B1 (7%), largely as previously described [16, 17]. In addition SYNE1 was mutated in 23% of cases, but did not reach significance by MutSigCV.

The high frequency of genomic catastrophes observed in our cohort was consistent with a significant role of larger-scale events in this disease - chromothripsis: 39/129 patients (30%), kataegis: 40/129 (31%), complex rearrangement events: 41/129 (32%), (Methods, Fig. 1f and Supplementary Fig. 4-7). The complex rearrangements included: focal amplifications with BFB pattern (11/129, 9%); focal amplifications <5Mb-wide with irregular copy number amplification steps (26/129, 20%); focal amplifications 5-10 Mb-wide with symmetric copy number amplification steps (10/129, 8%); double minute-like patterns (3/129, 2%); and subtelomeric BFBs (1/129, 1%) (Supplementary Fig. 7). The chromothripsis and BFB/complex rearrangement event frequencies were in a similar range to that described by Nones et al [18] - 33% and 27%, respectively. Kataegis rates were lower than that previously reported (19/22 = 86%), likely due to our more stringent criteria for calling (Methods). An enrichment of C>T and C>G mutations was observed in kataegis regions, as previously reported [25] (Supplementary Fig. 5).

Hence, this is a heterogeneous cancer dominated by copy number alterations and large scale rearrangements. Clinically meaningful genomic subgroups relevant for therapy are not immediately apparent from these analyses.

Receptors and downstream RTK targets are pervasively disrupted in EAC

Next we examined the genomic data to understand possible reasons for the disappointing results seen with many of the trials targeting growth factor receptors. Resistance to RTK therapy generally results from co-amplifications of alternative RTKs or amplification/activation of downstream mitogenic pathways. In our cohort we observed widespread gene amplification across multiple RTKs, as well as within the MAPK and PI3K pathways. Such patterns were similar among endoreduplicated and non-endoreduplicated samples, as well as in a panel of cell models (Fig. 2a, 2b).

When considering high level amplifications (GISTIC cut-off greater than 2), we report similar rates to those reported previously for EGFR and HER2 [26, 27]. HER2 was the most amplified RTK (22/129 patients = 17%), followed by EGFR (14/129 patients =

11%). Other commonly over-expressed RTKs included MET and FGFR. All these receptors are targeted in clinical trials with ongoing recruitment [28]. When considering lower level amplifications across these RTKs and downstream signaling pathways (GISTIC >1), these are highly prevalent and may still have biological significance accounting for disappointing trial results.

We used microarray expression data for available cases to check the consequences of the observed gains/losses at the transcriptional level for key amplified genes. The genes falling in amplified/gained regions show an increased expression compared to those in lost/deleted regions, confirming the observations from the WGS data (Fig. 2c). This, together with results from IHC staining of matched cases, suggests phenotypic relevance of the genome-level findings (Fig. 2d).

Overall, 40% of the samples have both receptor gain and downstream activation of at least one gene, 43% RTK gain alone, and a small number (2%) have downstream activation alone (Fig. 2e). We only see a single RTK gain, without gains or amplifications in the MAPK or PI3K pathways, in 9% of tumors, and in these cases, the RTKs involved are EGFR (4), ERBB2 (3), ERBB3 (1), FGFR1 (1), FGFR3 (1) and MET (1). The observed co-amplification patterns are unlikely to be biased by locus positioning, as the inspected RTKs have a varied distribution on chromosomes, so the co-amplifications in these genes appear to be selected for.

We therefore surmised that tailored RTKi combination therapy might be beneficial in some cases and decided to explore this in *in vitro* model systems. Since copy number gain events were seen most commonly in ERBB2, EGFR, MET and FGFRs, a panel of small molecular inhibitors was selected to target these RTKs. As expected, a single agent did trigger a cytotoxic effect in cell lines with a gain at that locus, but only in the micromolar range (Fig. 2g). In cell lines with an ERBB2 and a MET amplification, a significant reduction in cell proliferation was observed when both RTKs were inhibited with a GI50 down in the nanomolar range, for example OE33 (Fig. 2f, 2g, Table 1). A similar finding was observed in Flo (EGFR/MET copy gain) and OAC-P4C (ERBB2/FGFR2 amplification) when treated with EGFRi/METi and ERBB2i/FRFGi combinations, respectively. Taken together, these results suggest that a combination of RTK inhibitors tailored to the amplification profile might offer a clinical therapeutic strategy. Nevertheless, the complexity and diffuse patterns of these alterations provide a distinct challenge in the stratification of patients for therapy.

Mutational signatures uncover distinct etiology in EAC

In view of the heterogeneity and RTK-resistance mechanisms, we sought alternative therapeutic insights into the data using mutational signature analysis in a three-base context via the non-negative matrix factorization (NMF) methodology described by Alexandrov et al [29]. We also used the recently described pmsignature [30] and SomaticSignatures [31] for comparison. These methods are based on different statistical frameworks and therefore some differences are to be expected; nevertheless the same key signature patterns were observed with similar-sized patient subgroups expressing the dominant signature types (Supplementary Notes, Supplementary Fig. 9-12). Six signatures were prominent (Supplementary Fig. 13-14): S17, the hallmark signature of EAC [16, 17] dominated by T>G substitutions in a CTT context and possibly associated with gastric acid reflux – here renamed S17A; a previously uncharacterized variant of this signature combining a relatively higher frequency of T>C substitutions with the classical T>G pattern found in S17, which we call S17B; S3, a complex pattern caused by

defects in the BRCA1/2-led homologous recombination pathway; S2, C>T mutations in a TCA/TCT context, an APOBEC-driven hypermutated phenotype; S1, C>T in a *CG context, associated with aging processes; and an S18-like signature, C>A/T dominant in a GCA/TCT context, formerly described in neuroblastoma, breast and stomach cancers (Fig. 3a). The exploration of a seven-base signature context using pmsignature yielded an A/T base dominance at the -3 and -2 positions for the S17 signature, but no other striking preferences for particular nucleotide combinations at the 2nd and 3rd bases for any of the other signatures (Supplementary Fig. 15). Overall, this suggests that the bases immediately adjacent to the position where the mutation occurs exert the main bias, with a potentially more complex mechanism for the S17 signature.

When considering the dominant mutation signatures on a per-patient basis, three subgroups of patients became apparent: *C>A/T dominant* (age, S18-like), *DNA Damage Repair (DDR) impaired* (BRCA), and *mutagenic* (predominantly S17A or S17B) (Fig. 3a). We chose the descriptor *mutagenic* because the mutation rate was significantly higher in this subgroup (Welch's t-test $p=0.0007$; Supplementary Fig. 16). The robustness of the subgroups was ensured through consensus clustering and confirmed by silhouette statistics (Methods, Supplementary Fig. 17-18). We have also validated our findings in an independent cohort of 87 samples [18] and show that: when we apply the NMF method the same dominant signatures (S1, S2, S3, S17, S18-like) are observed; and when we perform clustering three subgroups emerge and these are of similar composition and proportions to those seen in the original cohort (Methods, Fig. 3b compared with Fig. 3a). Furthermore, the total mutational burden is again consistently higher in the mutagenic subgroup of the validation cohort. No cellularity bias or batch effect was observed among subgroups (Supplementary Fig. 19).

To test whether spatial sampling might have induced a bias in the predicted signatures, we inspected three additional patients who had multiple samples taken. The mutational patterns showed remarkable consistency across all three biopsies, especially with respect to the dominant signature (Fig. 3c). This suggests that, despite the heterogeneity of this disease, the mutational signature analysis should be sufficiently robust to cope with spatial sampling bias.

We next examined whether the defined subgroups presented similarities in terms of genomic characteristics. All three subgroups showed a similar degree of heterogeneity in copy number alterations by chromosomal arm (Supplementary Fig. 20), and the RTK co-amplification profiles were fairly similar among subgroups (Supplementary Fig. 21). Of note, the C>A/T dominant subgroup had a two-fold higher frequency of ERBB2/MET co-amplifications, but this did not reach statistical significance.

The rearrangement patterns in the three subgroups denoted differences in genomic stability. In particular, unstable genomes were less frequent in the C>A/T dominant subgroup and most frequent in the DDR impaired subgroup, as defined by the structural variant (SV) based classification [11, 18] (Supplementary Fig. 22). When examining SV signatures in a similar manner using the NMF framework (Methods), the C>A/T dominant subgroup also had lower levels of large-scale duplications and an increased frequency of focal interchromosomal translocations, which suggest mobile element insertion events (Supplementary Fig. 23). The DDR impaired subgroup seemed to have the largest degree of genomic instability, even though SV signatures were overall rather heterogeneous. No recurrently altered genes (in >10% of the cohort) were over-represented in any of the three subgroups after multiple testing correction, nor were there any differences in TP53 or HER2 status among the subgroups to account for the differences in genomic stability.

The clinical characteristics of the three subgroups did not differ significantly (Supplementary Table 5, Supplementary Fig. 24), implying that the classification, and hence spectrum of mutation patterns, does not vary with smoking, age, sex, tumor histopathological grade, tumor stage, response to chemotherapy, overall or recurrence-free survival etc. Hence, the mutation signature profiles seem to be capturing a different type of information compared with current clinical classification methods.

Evidence of DNA damage repair deficiency in EAC

Next we investigated what aspects of the DNA damage response were defective in the DDR impaired subgroup. Although a BRCA signature was recovered, there were only 3 nonsynonymous mutations and 3 germline variants (non-intronic) in either BRCA1 or 2 in a total of 5 out of 18 patients, suggesting that other mechanisms were largely responsible for this signature (Supplementary Tables 6 and 7). We thus assessed the mutational rates across more than 450 genes associated with DDR, as previously described in a pan-cancer analysis [32] (Fig. 4, Methods). We found that there was a 4.3-fold enrichment of samples with alterations in homologous recombination (HR) pathways in the DDR impaired subgroup compared to the others (95% CI [1.47, 12.56]). It is therefore likely that a pathway-level disruption of HR contributes to the BRCA-like mutational signature rather than mutations of BRCA genes.

The analysis of DDR genes in the whole cohort unsurprisingly showed that the most mutated pathway was TP53 (Supplementary Fig. 25), and this was consistent among subgroups (Fig. 4a), as were the amplification and deletion patterns (Supplementary Fig. 26). In addition, more than 24% of the genomes had defects in chromatin remodelling, comprising recurrently mutated genes like ARID1A (8%) and SMARCA4 (8%) (Fig. 4b). ARID1A is also recruited to DNA double strand breaks (DSB), where it facilitates processing to single strand ends [33]. Defects in ARID1A impair this process and sensitise cells *in vitro* and *in vivo* to PARP inhibition (PARPi) [33].

Neoantigen burden coupled with etiological differences suggest new therapeutic avenues

Modulation of the cytotoxic T cell response using monoclonal antibodies against the Programmed Death Receptor or Ligand (PD-1 and PD-L1 inhibitors), as well as those targeting CTLA4 (Ipilimumab) have shown promise in the treatment of solid tumors [34-36]. The recent literature suggests that both numbers of mutations and total neoantigen burden have been coupled with significantly better clinical responses to immunotherapy [37-39].

We found that the mutagenic subgroup, whose observed signature may be due to gastric acid reflux, harboured a significantly higher nonsynonymous mutational burden, as well as higher levels of neoantigen presentation (Welch's t-test $p=0.0007$ and Wilcoxon rank-sum test $p<<0.0001$, respectively; Fig 5a and Supplementary Fig. 16). This is in keeping with that observed for lung cancer and metastatic melanoma, with a 1.5-fold higher median neoantigen burden in this subgroup versus the rest – similar to the two-fold ratio reported by Rizvi et al [37, 40]. Using available microarray expression and RNA-Seq data, we observed a significantly higher number of neoantigens expressed in the mutagenic subgroup compared to the rest (Wilcoxon rank-sum test p -value = 0.042, Fig. 5a).

In recent studies, an enriched population of pre-existing CD8+ T cells was shown to predict a favorable outcome from PD-1 blockade therapy [41, 42]. We found a higher density of CD8+ T cells in a subset of available samples from the mutagenic signature subgroup compared with samples from the other subgroups (Fig. 5a, 5b).

Treatment responses in mutational signature subgroups

Given the complexity of the RTK landscape and the apparent need to profile each patient to determine the optimal combination of RTK inhibitors, we hypothesised that the more homogeneous profile of mutational signatures - yet with discernable differences between the three subgroups in terms of mutation frequency and DDR pathways - might be a more clinically applicable starting point to guide therapy decisions. To start to test this hypothesis, we used newly derived cell line models from patients in the OCCAMS consortium with an available germline reference sequence from which we could derive the signatures: OES127, DDR impaired profile; MFD, mutagenic profile; AH277, C>A/T dominant profile (Fig. 6a). For the DDR impaired profile we hypothesised that PARPi, with or without a DNA-damaging agent such as Topotecan, might be beneficial [33, 43, 44]. Topoisomerase I (Topo1) is an enzyme required for DNA replication and when inhibited in combination with Olaparib it has been shown to generate synthetic lethality in BRCA deficient cases [45, 46]. No cytotoxic effect was observed when Olaparib or Topotecan was used as single reagent, however, a marked synergistic effect was shown when Topotecan was combined with Olaparib for OES127 (DDR impaired group), but not for the other primary cell lines (Fig. 6b, Supplementary Table 8).

Next we were interested to test the efficacy of Wee1/Chk1 inhibitors given the high frequency of p53 mutation in this disease [47, 48]. Several recent studies revealed that pharmacological inhibition of G2/M-phase checkpoint regulators Wee1 and Chk1/2 resulted in an antitumorigenic effect in some highly mutated cancers [49, 50]. We therefore hypothesised that inhibition of mitotic checkpoints would be cytotoxic in EAC and that this might be more apparent in cells with a high mutation burden [51, 52]. As expected, a cytotoxic effect for these drugs was observed to some extent in all of our primary cell lines, but the sensitivity was increased in the AH277 and MFD lines in comparison with the p53 WT line OES127 (Fig. 6c, Supplementary Table 9). In the MFD cells with a mutagenic signature, there was a 25-fold and 10-fold increased sensitivity in response to the Wee1 and Chk1/2 inhibitor, respectively, compared with the AH277 cells from the C>A/T dominant subgroup.

These experimental data provide a starting point from which to evaluate therapeutic options derived from mutational signatures, especially as primary model systems more closely resembling human disease and with stromal components become available [53, 54].

DISCUSSION

Whole-genome sequencing of 129 EAC patients has unveiled a high prevalence of large-scale alterations that may play an important role in the development of this cancer. Similarly to ovarian, breast and lung cancers which have been described as 'copy number driven' [55], relatively few genes were recurrently point-mutated (except TP53), but there were frequent recurrent amplifications in sites harbouring oncogenes,

deletions of important cell cycle components (CDKN2A, CDKN2B) and rearrangements of genes like RUNX1, frequently translocated in leukemias [56]. The highly heterogeneous landscape of potential genomic drivers explains the difficulties encountered to date in finding suitable avenues for tailored therapies. 88/262 registered esophageal trials [28, 57] target RTKs and mitogenic signalling pathways with remarkably little clinical efficacy. The genomic and *in vitro* analyses of EAC cell lines performed here suggest that the high prevalence of co-amplification of RTKs and downstream mitogenic pathway genes is a likely cause for these disappointing results.

Although all six mutational signatures are seen to a greater or lesser extent in most patient tumors, three distinct dominant subtypes, namely *DDR impaired*, *C>A/T dominant*, and *mutagenic*, point to specific etiological factors or genetic instabilities dominating the development of any individual's EAC. We hypothesise that the insights obtained from mutational signatures could be harnessed for future studies that might investigate the potential of using tailored therapies to complement the current treatment options as summarized in Figure 7.

In the DDR impaired subgroup with an enrichment for HR dysfunction, a synthetic lethality approach may prove useful. Indeed, HR scarring is a good a biomarker for the purposes of DDR targeted treatment [58], being well established in breast and ovarian cancer and more recently also reported in gastric tumors [59]. HR dysfunction renders tumors sensitive to platinum-based chemotherapy and PARPi, which has started to make a survival impact in other BRCA-related tumors [60]. Indeed, we also observe some increased sensitivity to platinum-based chemotherapy in the DDR impaired subgroup in our cohort (Supplementary Fig. 27). PARPi in combination with irradiation has shown to be potent in HR scarred tumors [61] and our data from a primary line with a DDR signature suggests that PARPi in combination with a DNA damaging agent might be beneficial.

Expression of PD-L1 has been demonstrated in gastroesophageal tumors at all stages, and as such, PD-L1 based immunotherapy might be an an attractive therapeutic avenue needing further exploration in this disease [62]. Both the nonsynonymous mutation burden and the neoantigen level, as well as CD8+ cell infiltration, have been shown to be good genomic biomarkers in predicting response to immunotherapy in both smoking-related non-small cell lung cancer and melanoma [37, 38, 42, 62]. In keeping with these other tumors which result from chronic exposure to mutagens (smoking and UV irradiation, respectively), we observe similar features in our mutagenic cohort containing an 'acid' signature. This type of genomic classification has also been proposed in other tumor types for patient stratification for immunotherapy [63] and warrants further investigation in this cancer. Similarly, Chk/Wee1 inhibitors may be promising tools for future studies in highly mutated, p53-inactive tumours [49, 50].

Patients in the C>A/T dominant subgroup would continue to be treated with conventional chemotherapy until more progress is made, for example with synthetic lethality approaches combined with radiotherapy or mutant TP53 reactivating drugs [64-66]. Alternatively, combined RTK inhibitors (especially ERBB2 and MET, given their prevalence in this subgroup) may be beneficial and combined MEK and Akt inhibition might be worthy of consideration given the low levels of amplifications/activation seen downstream in the MAPK and PI3K pathways [67].

One practical question that arises is how this approach could be implemented clinically. Despite the decreasing costs of WGS, it is still expensive and signatures are problematic to derive from whole-exome data [29]. However, lower coverage whole-genome (10x), or even shallow (1x) genome sequencing could provide a cost-effective,

high-throughput alternative for signature-based stratification and we have shown using simulations down to 10x that we can confidently retrieve dominant signatures at lower coverage (Supplementary Fig. 28). Moreover, while designing custom gene panels would pose serious difficulties in such a heterogeneous disease, mutational signature-based classification would enable us to bypass the tumor heterogeneity bottleneck by providing a genome-wide, spatially-independent classification strategy (Fig. 3c).

For subsequent classification of individual patients, we propose using a quadratic programming approach whereby we predict exposures to the six mutational signatures without having to estimate a large set of parameters (as with the classical NMF algorithm) and use the dominant signature pattern for patient assignment (Methods). The example in Figure 7, performed for newly derived ICGC data, illustrates this fast and effective way of classifying new patients. This methodology is of course not without limitation: the age, S18-like and APOBEC signatures are currently grouped together, but in a much larger cohort a distinct 'age' or 'APOBEC' subgroup might emerge, with their own characteristics. Similarly, signatures S17A and S17B may merge into a single signature in a much larger cohort, as was the case for signatures S1A and S1B [29]. It should be borne in mind that algorithms for defining signatures are evolving with improved speed of computation [30] and there is inherent variation in sample categorization between methods. Methodology is also being developed to accurately identify signatures de-novo in single patients, which we expect will offer a promising alternative for patient stratification.

In summary, we have uncovered possible reasons for the lack of efficacy in molecularly targeted trials thus far, and present a novel genomic classification of these tumors which links etiology to patient stratification with potential therapeutic relevance. Further studies will be needed for pre-clinical validation prior to implementation in trials, as well as to understand the extent to which this genomic distinction is maintained downstream, at the level of the transcriptome, proteome and cellular phenotype.

METHODS

Ethical approval, sample collection and DNA extraction

The study was registered (UKCRNID 8880), approved by the Institutional Ethics Committees (REC 07/H0305/52 and 10/H0305/1), and all subjects gave individual informed consent. Samples were obtained from surgical resection or by biopsy at endoscopic ultrasound. Blood or normal squamous esophageal samples at least 5 cm from the tumor were used as a germline reference. All tissue samples were snap frozen at collection and stored at -80°C . Before DNA extraction, one section of the sample was stained with hematoxylin and eosin and sent for cellularity review by two expert pathologists. Cancer samples with a cellularity $\geq 70\%$ were submitted for whole-genome sequencing. DNA was extracted from frozen esophageal tissue using the AllPrep kit (Qiagen) and from blood samples using the QIAamp DNA Blood Maxi kit (Qiagen).

A total of 129 cases (matched tumor-normal) were sequenced and analyzed in the study. True esophageal and gastroesophageal (GOJ) type 1 and 2 tumors (according to Siewert classification) were used. All GOJ type 3 tumors (14 in total) were excluded from the analysis. This sample size constitutes a considerable increase from earlier WGS studies in this cancer [16, 17] and is of similar size to whole-exome studies reported to date [16, 17], with the advantage of covering the full genome. It is expected, therefore,

that it should present enough power to detect a similar number of significant somatic events affecting genes, and an increased power to depict the landscape of larger scale alterations in EAC.

Whole-genome sequencing analysis

Whole-genome sequencing was performed on a tumor and matched normal sample for each patient in the cohort. A single library was created for each sample, and 100-bp paired-end sequencing was performed under contracts by Illumina and the Broad Institute to a typical depth of at least 50x for tumors and 30x for matched normals, with 94% of the known genome being sequenced to at least 8x coverage and achieving a Phred quality of at least 30 for at least 80% of mapping bases. Read sequences were mapped to the human reference genome (GRCh37) using Burrows-Wheeler Alignment (BWA) 0.5.9 [68], and duplicates were marked and discarded using Picard 1.105 (<http://broadinstitute.github.io/picard>). As part of an extensive quality assurance process, quality control metrics and alignment statistics were computed on a per-lane basis.

The FastQC package was used to assess the quality score distribution of the sequencing reads and perform trimming if necessary.

Samples were examined for potential microsatellite instability (MSI) using computational tools, and five cases with potential MSI were subsequently excluded from the analysis, as previously performed in other studies [16] (Supplementary Notes and Supplementary Table 10).

Somatic mutation and indel calling

Somatic mutations and indels were called using Strelka 1.0.13 [69]. SNVs were filtered as described in Supplementary Table 11. Functional annotation of the resulting variants was performed using Variant Effect Predictor (VEP release 75) [70].

Significantly mutated genes were identified using MutSigCV [24].

Copy number and loss of heterozygosity analysis

For patient-derived samples, absolute genome copy number after correction for estimated normal-cell contamination was called with ASCAT-NGS v2.1 [71], using read counts at germline heterozygous positions estimated by GATK 3.2-2 [72].

Cellularity, expressed as the relative proportion of tumor and normal nuclei, was also obtained using ASCAT. It was distributed as follows: 18% of samples had cellularity <0.3; 71% of samples between 0.3 and 0.7; 11% of samples ≥ 0.7 .

Significantly amplified/deleted regions in the cohort were identified using GISTIC2.0 [23], after correcting the copy numbers for ploidy (total copy number of the segment divided by the average estimated ploidy of each sample). GISTIC2.0 was run on an input defined as the log₂ of such corrected copy number values, with gain (-ta) and loss (-td) thresholds of 0.1 and sample centering prior to analysis. Copy number change thresholds considered for downstream analysis were: amplifications, GISTIC score ≥ 2 ; deletions, ≤ -2 . Loss of heterozygosity (LOH) was defined as ASCAT-estimated minor allele copy number of 0.

A whole-genome duplication event was considered to have occurred in a sample if the average estimated ploidy by ASCAT was ≥ 3 , similar to the cut-offs suggested in [73].

For cell lines, copy number calling was performed using Control-FREEC [74].

RTK copy number profiling

To examine the landscape of copy number alterations in RTKs and downstream key genes (Fig. 2), a score from -2 to 2 was used to denote: deletions (-2), losses (-1), gains (+1), amplifications (+2). For the patient derived samples, copy numbers estimated using ASCAT were subsequently classified according to GISTIC2.0 using the same scoring scheme. For the cell models, a GISTIC-equivalent score was derived by dividing the estimated copy numbers by Control-FREEC by the average ploidy of each cell line, and classifying regions ≥ 2 as amplified (equivalent score=2), regions ≤ -2 as deleted (equivalent score=-2), and regions >1 or <1 as gained or lost, respectively (equivalent scores +1/-1). For the MFD line only the parent tumour was sequenced, so the copy numbers were inferred using ASCAT and GISTIC2.0 as described above.

In Figure 2b, the average copy number value of downstream key genes is highlighted for each representative gene (e.g. RAS summarizes the copy number landscape of HRAS, KRAS, NRAS), hence the scores take continuous rather than discrete values as in panel 2a.

Structural variant and mobile element insertion calling and annotation

Structural variants were called using BWA-mem for alignment [75], against the GRCh37 reference human genome, followed by clustering of putative breakpoint junctions identified by discordant read pairs and split reads using Manta [76]. We then discarded: SVs overlapping gaps, satellite sequences, simple repeats >1000 basepairs or extreme read depth regions; and deletions of < 1000 bp that were not supported by at least one split read defining the deletion junction. Small inversions up to 10 kb were also discarded as they are generated artefactually in some libraries [77]. Breakpoints in genes were annotated against Ensembl GRCh37, version 75 [18]. Fragile sites were annotated from Le Tallec et al [78].

SV calls that represented mobile element insertions—either because the mobile element transduced unique sequence or its polyA tail was mapped by the aligner [21]—were identified from lists in Paterson et al [21] and Tubio et al [22]. SVs likely to be additional mobile element transductions—extensions of known transduced sequence or sequences transduced by L1s that were not previously known to transduce—were also identified in the following way: (1) SVs were pooled from all tumors, and clusters of at least five interchromosomal breakpoint junctions within maximum 1 kb of each other identified; (2) from these, clusters harbouring five-fold more interchromosomal translocations than other types of SVs and where there were at least four different partner chromosomes to which the presumed transduced sequences were joined, were identified as likely additional mobile element transductions. Many were associated with known L1 polymorphisms [79]; as expected, around half had an SV at each end of the insert. This and increased sensitivity from using the BWA-MEM aligner considerably increased the number of SVs identified as inserts compared to [21].

When examining genes altered by SVs, a moderate correlation was found between the number of SVs affecting a gene and gene length (Pearson correlation coefficient = 0.4, Supplementary Fig. 29). To prioritize rearranged genes of potential impact in the cohort, we first performed the following filtering steps: (1) all annotated fragile sites were removed from the list of genes overlapping SVs; (2) to capture potential unannotated fragile sites, we scored all genes using the following scoring:

$S_{\text{gene}} = D_b \times N_p \times L_{\text{gene}}$, where D_b = total breakpoint density along the genome over all samples where breakpoints cause internal deletions in the gene (number of such breakpoints divided by the length of the genome), N_p = total number of patients where the gene presents internal deletions, and L_{gene} = length of the gene.

Genes with scores >10-fold higher than the 99% quantile over the full list were filtered out as likely fragile sites (Supplementary Table 12).

For the remaining set of genes, we scanned 100 kb windows along the genome, with 50 kb overlap, for hotspots of SV breakpoints (defined as breakpoint accumulations within the window) and prioritized the top 1% hotspots with highest breakpoint density. Genes harbouring at least one such hotspot and rearranged in more than 10% of the patients were selected as top hits of potential impact in this cancer.

Structural variant-based classification of genomes

The structural variant-based classification was used to annotate unstable, stable, locally rearranged and scattered genomes as previously described [11], but with different cut-offs for stable and unstable genomes, to account for the different genomic instability landscape in EAC compared to pancreatic cancer: genomes were deemed “stable” if the total number of SVs was less than the 5% quantile in the cohort, and unstable if the number of SVs exceeded the 95% quantile. The criteria for locally rearranged and scattered genomes were kept the same as previously described.

Mutational signature analysis

Discovery

Mutational signatures were identified using the NMF methodology described by Alexandrov et al [29]. Before running the software, common variants in the 1000 genomes database [80] appearing in at least 0.5% of the population were removed, and samples with cellularity <25% (from ASCAT estimates) were not included, leaving a total of 120 samples for the analysis. The optimal number of signatures in the dataset was chosen to balance the signature stability against the Frobenius reconstruction error (Supplementary Fig. 13). To increase confidence in the findings, two other methods were also used: the R packages *pmsignature* [30] and *SomaticSignatures* [31] (Supplementary Notes and Supplementary Fig. 9-12).

To establish which of the two C[T>G]T signatures resembled most the classical S17 signature recorded in the COSMIC database, we used the cosine similarity distance measure between the probability vectors of these signatures. The signature which we termed S17A had a higher cosine similarity distance compared to S17B (0.98 versus 0.92), and we hence considered it to be more reflective of the signature reported in the literature.

Samples in the discovery cohort were clustered by their signature exposures using a consensus clustering approach [81] (based on Pearson correlation distance with complete linkage) in order to increase the robustness of the subgroup assignment.

Validation

The three mutational signature subgroups were validated in an independent cohort of 87 EAC samples (21 from [18] and 66 independent patients in our ICGC study post-neoadjuvant therapy and surgery). These had been selected from a slightly larger cohort after removing low cellularity and MSI positive samples. Within the validation cohort,

the same dominant signatures were inferred using the NMF method, as above. The signature contributions were estimated based on the six main processes inferred in the test cohort using quadratic programming (described later in the Methods).

Multiple sampling

To test the differences in mutational exposures coming from three different spatial locations within the same sample, we have used three available cases for which multiple samples had been collected from the same tumour. We obtained the mutational exposures for the six described signatures using quadratic programming.

Structural variant signature analysis

Similar to inferring mutational signatures, we used the methodology by Alexandrov et al [29] to discover structural variant signatures in EAC genomes. We classified structural variants (deletions, inversions, insertions, interchromosomal translocations) by their size and distribution along the genome. SVs were grouped by size into “small” and “large”, defined with respect to the 25% quantile length in the cohort for the respective SV type). To determine the SV distribution along the genome, we assessed the degree of clustering within 10 Mb windows along the genome. If the SV of interest fell within a window of clustered events (where the total number of SVs exceeded 1.5x the 75% quantile of the total number of events in that genome), then it was deemed a “focal” event. Otherwise, it was catalogued as “genomically distributed”. These characteristics defined a total of 14 features to be used for signature discovery (Supplementary Fig. 23).

Identification of catastrophic events

Kataegis was called in a similar manner to Nones et al [18], by calculating the distance between consecutive mutations and segmenting the resulting genome-wide signal using piecewise constant fitting as implemented in the *copynumber* Bioconductor package [82] (Supplementary Fig. 5). However, acknowledging that the intermutational distance distribution varies from genome to genome, we did not use a fixed cutoff of 1000 bases for the mean distance between mutations in kataegis loci, but instead applied a variable cutoff that was determined as the 1% quantile of the intermutational distances within the respective genome.

Chromothripsis events were identified in chromosomes containing >10 CN steps, according to the criteria described by Korbel and Campbell [83] and Nones et al [18]: (a) clustering of breakpoints; (b) regularity of oscillating CN steps; (c) interspersed loss and retention of heterozygosity; (d) randomness of DNA segment order and fragment joins; (e) ability to walk the derivative chromosome. Scripts were developed to assess these criteria, and the final chromothripsis calls were prioritized through visual inspection (Supplementary Fig. 6).

Regions of clustered inversions were identified as a proxy for BFB and complex rearrangement events. These were defined by scanning for enrichments of inversions (1.5x the upper quantile of the total number of events in the genome) within 5-Mb windows throughout the genome. Visual inspection was used to prioritize those regions that displayed BFB-like characteristics. Several types of complex rearrangement events were identified: focal amplifications with BFB pattern (clustered inversions along with progressive amplification steps primarily on one side of the inversion cluster, i.e. asymmetric); other focal amplifications within narrow regions <5 Mb (clustered

inversions coupled with copy number amplifications displaying an irregular pattern), focal amplifications within wider 5-10 Mb regions (clustered inversions and progressive copy number amplification steps, often with multiple peaks); double minute-like patterns (clustered inversions at high copy number amplification regions without evidence of a progressive mechanism); potential subtelomeric BFBs (amplifications located close to the ends of the chromosomes, coupled with inversion clusters and distal deletions). See Supplementary Figure 7 for sample illustrations of the patterns described.

DNA damage repair (DDR) analysis

To assess the alterations in DNA damage-related pathways, we performed an analysis similar to the one described by Pearl et al [32]. Among the genes involved in defined DNA damage pathways as described in the paper, we only selected those affected more often than the expected background of synonymous mutations, similar to the method described by Puente et al [84]. The probability of a gene being affected by M nonsynonymous mutations in the cohort follows a poisson binomial distribution and is calculated relative to a basal probability depending on the number of nonsynonymous (n_{ns}) and synonymous (n_s) mutations, gene size (L), local mutational density for the locus (d) and total length of coding regions in the genome (E) as follows:

$$P_{ns} = \frac{n_{ns}Ld}{(n_{ns} + n_s)E}$$

Subsequently, we catalogued those that harboured nonsynonymous somatic mutations/indels with possible deleterious effect (as predicted by SIFT [85]/PolyPhen [86]) or copy number alterations (amplifications and deletions using the defined GISTIC cut-offs) in our cohort. We then compared the mutational load in 16 main pathways among the defined mutational signature subgroups.

Neoantigen predictions and analysis

In order to quantify the neoantigen load in the tumors, we performed the analysis as described in [37]. We first collected all peptides defined by a 17 amino-acid region centered on the amino acid which changes upon the mutation. We identified mutant nonamers with ≤ 500 nM binding affinity for patient-specific class I human lymphocyte antigen (HLA) alleles, constituting potential candidate neoantigens. Binding affinities were predicted using NetMHC-3.4 [87]. We then quantified the peptides that displayed high affinity binding in tumor, but low or no binding in the respective matched normal and obtained total counts for each defined mutational subgroup. The neoantigen burden in tumours belonging to the different subgroups varied as follows: DDR impaired – an average of 77 (s.d. = 42.2); C>A/T dominant – an average of 86 (s.d. = 41.3); mutagenic – an average of 111 (s.d. = 43.9). The three groups presented unequal variance in terms of nonsynonymous mutation burden, as shown by pairwise F-tests ($p < 0.05$ after multiple testing correction using the Benjamini-Hochberg method). To adjust for this, the mutation burden among subgroups was compared using Welch's t-test. The neoantigen load, on the other hand, had similar variance between the mutagenic group and the other two groups combined (F-test $p > 0.05$), so the Wilcoxon rank-sum test was used to compare the predicted neoantigen presence in tumors.

To verify that the predicted neoantigens were indeed expressed in the samples, microarray and RNA-Seq derived expression Z-scores were investigated and all peptides with a score higher than the average in the respective sample were considered expressed.

Microarray expression profiling

Purified Total RNA was extracted using the AllPrep DNA/RNA Mini Kit from Qiagen. Quality of RNA was assessed using the NanoDrop and the Agilent Bioanalyser, and only samples with RIN>7 were accepted for microarray or RNA-Seq. The Illumina HTv4.0 beadchip was used as platform for expression analysis. Bead level readings were corrected for spatial artefacts and the signal per probe ratio was computed. Relative array weights were applied before quantile normalization for gene expression analysis.

For the validation of RTK gains/losses and neoantigen expression, available microarray data for a total of 42 samples were used. To evaluate expression levels for selected genes, Z-scores were obtained relative to the average expression in the sample or of the specific investigated gene.

RNA sequencing and analysis

Purified total RNA was subject to ribosomal depletion using methods already published [88]. In brief, 195 DNA oligonucleotides (Sigma Life Sciences) were pooled together in equal molar amounts and incubated with total RNA Hybridase Thermostable RNase H (Epicentre). RNaseH-treated RNA was purified using 2.2x RNAClean SPRI beads (Beckman Coulter LifeSciences) and oligonucleotides removed using TURBO DNase rigorous treatment. A further purification of the DNase-treated RNA with 2.2x RNAClean SPRI beads was followed by library preparation using the TruSeq HT Stranded mRNA kit according to the manufacturers instructions (Illumina) and generated single end reads using the HiSeq 2500.

For the validation of neoantigen expression, available RNA-Seq data for a total of 18 samples were used. To evaluate expression levels for selected genes, Z-scores were obtained relative to the average expression in the sample.

Cell lines and reagents

The primary cell line panel was derived from EAC cases included in the ICGC sequencing study, including MFD (Tim Underwood, Southampton, OCCAMS consortium member), OES127 (Anna Grabowska, Nottingham, OCCAMS consortium member) and AH277 (organoid, Mathew Garnett, Cambridge). The MFD line required 10% fetal calf serum (PAA) in DMEM medium (Invitrogen, ThermoFisher Scientific) and the AH277 culture method was as previously described [53]. The feeder layer system was used to expand OES127 lines. The established EAC lines, SK-GT-4, OAC-P4C, OACM5.1C, and OE33 were cultured in RPMI medium (Sigma) with 10% fetal calf serum, except for Flo, which was grown in DMEM with 10% fetal calf serum. The identity of all cell lines was verified by short tandem repeat (STR) profiling. All cells were routinely examined for mycoplasma contamination.

Small molecular inhibitors used for treatment were: Lapatinib, AZD-4547, Olaparib, MK-1775 and AZD-7762 (BioVision), Crizotinib (LKT Labs) and Topotecan (Cayman Chemical). Inhibitors were diluted to working concentrations in DMSO (Sigma).

Immunohistochemistry

Sections of 3.5 μm were stained by a Bond Max autostainer according to the manufacturer's instruction (Leica Microsystems). Primary antibodies ERBB2 (1:300, Cell Signaling Technology), MET (1:300, Cell Signaling Technology), CD8 (1:100, Dako) were optimised and applied with negative controls.

CD8+ cells were counted manually in two tumour areas of 1 mm^2 each (except in one case where there was sufficient material for one count only) and an average was calculated.

Drug sensitivity assays

The seeding density for each line was optimised to ensure cell growth in the logarithmic growth phase. Cells were seeded in complete medium for 24 hours then treated with compounds at 4-fold serial dilutions for 72 hours. Cell proliferation was assessed using CellTiter-Glo (Promega). The anchor inhibitors were kept constant at 1M in combination studies.

The concentrations of a compound causing 50% growth inhibition relative to the vehicle control (GI50) were determined by nonlinear regression dose-response analysis and the area under the curve (AUC) was calculated using GraphPad Prism.

Proposed approaches to classifying new patients

Classification of new patients based on their mutational signatures could be performed in either of the following ways:

1. By examining the mutational exposures to signatures after running the sample together with a defined panel of tumors (currently, the 120 sample cohort) through the NMF pipeline.
2. By fitting the mutational counts in the respective genome to a model defined based on the mutational probabilities (as recorded in the COSMIC database) for the six oesophageal signatures using quadratic programming. Quadratic programming is well suited for this type of problem, as it tries to optimize the signature exposures under the constraint that they should add up to one.

The advantage of the latter approach is that it reduces the problem to a linear one, and thus the computation time is dramatically reduced. Moreover, no pre-defined panel of samples is needed for the method, only the expected distribution of nucleotide substitutions for the mutational signatures of interest (obtained from COSMIC or from the initial outcomes using the NMF pipeline).

We model the observed mutation count vector Y (96 possible contexts) on the six mutational signature processes α_j discovered as follows:

$$Y = \alpha_1 S_1 + \alpha_2 S_2 + \alpha_3 S_3 + \alpha_4 S_4 + \alpha_5 S_5 + \alpha_6 S_6 + Y_{\text{noise}}$$

with $\sum_j \alpha_j = 1$ and $\alpha_j \geq 0$. We minimize

$$\sum_i (Y_i - (\sum_j \alpha_j S_{ij}))^2$$

subject to these constraints, where $i=1..N$ signatures and $j=1..M$ contexts.

Statistics

All statistical tests were performed using a Wilcoxon rank-sum test or ANOVA (for continuous data), and a Fisher exact test or Chi-square test (for count data). Welch's t-test was used when comparing groups of unequal variance. Multiple testing corrections were performed where necessary using the Benjamini-Hochberg method. All reported p-values were two-sided.

Code availability

The scripts used to perform the analysis are available upon request.

Accession codes

The whole-genome sequencing data can be found at the European Genome-phenome Archive (EGA) under accession EGAD00001001457.

ACKNOWLEDGEMENTS

Whole-genome sequencing of esophageal adenocarcinoma samples was performed as part of the International Cancer Genome Consortium (ICGC) through the oEsophageal Cancer Clinical and Molecular Stratification (OCCAMS) Consortium and was funded by Cancer Research UK. We thank the ICGC members for their input on verification standards as part of the benchmarking exercise. We thank the Human Research Tissue Bank, which is supported by the National Institute for Health Research (NIHR) Cambridge Biomedical Research Centre, from Addenbrooke's Hospital and UCL. Also the University Hospital of Southampton Trust and the Southampton, Birmingham, Edinburgh and UCL Experimental Cancer Medicine Centres and the QEHB charities. This study was partly funded by a project grant from Cancer Research UK. R.C.F. is funded by an NIHR Professorship and receives core funding from the Medical Research Council and infrastructure support from the Biomedical Research Centre and the Experimental Cancer Medicine Centre. We acknowledge the support of The University of Cambridge, Cancer Research UK (C14303/A17197) and Hutchison Whampoa Limited. We would like to thank Dr. Peter Van Loo for providing the NGS version of ASCAT for copy number calling. We are grateful to all the patients who provided written consent for participation in this study and the staff at all participating centres.

Some of the work was undertaken at UCLH/UCL who received a proportion of funding from the Department of Health's NIHR Biomedical Research Centres funding scheme. The views expressed in this publication are those of the authors and not necessarily those of the Department of Health. The work at UCLH/UCL was also supported by the CRUK UCL Early Cancer Medicine Centre.

COMPETING FINANCIAL INTERESTS

The authors declare no competing financial interests.

References

1. Ferlay, J., et al., *Cancer incidence and mortality worldwide: sources, methods and major patterns in GLOBOCAN 2012*. International Journal of Cancer, 2015. **136**(5): p. E359-86.
2. Brown, L.M., S.S. Devesa, and W.H. Chow, *Incidence of adenocarcinoma of the esophagus among white Americans by sex, stage, and age*. J Natl Cancer Inst, 2008. **100**(16): p. 1184-7.
3. Cunningham, D., A.F. Okines, and S. Ashley, *Capecitabine and oxaliplatin for advanced esophagogastric cancer*. N Engl J Med, 2010. **362**(9): p. 858-9.
4. Allum, W.H., et al., *Long-term results of a randomized trial of surgery with or without preoperative chemotherapy in esophageal cancer*. J Clin Oncol, 2009. **27**(30): p. 5062-7.
5. Cunningham, D., et al., *Perioperative chemotherapy versus surgery alone for resectable gastroesophageal cancer*. N Engl J Med, 2006. **355**(1): p. 11-20.
6. van Hagen, P., et al., *Preoperative chemoradiotherapy for esophageal or junctional cancer*. N Engl J Med, 2012. **366**(22): p. 2074-84.
7. Bang, Y.J., et al., *Trastuzumab in combination with chemotherapy versus chemotherapy alone for treatment of HER2-positive advanced gastric or gastro-oesophageal junction cancer (ToGA): a phase 3, open-label, randomised controlled trial*. Lancet, 2010. **376**(9742): p. 687-97.
8. Gao, Y.B., et al., *Genetic landscape of esophageal squamous cell carcinoma*. Nat Genet, 2014. **46**(10): p. 1097-102.
9. Schulze, K., et al., *Exome sequencing of hepatocellular carcinomas identifies new mutational signatures and potential therapeutic targets*. Nat Genet, 2015. **47**(5): p. 505-11.
10. *Genomic Classification of Cutaneous Melanoma*. Cell, 2015. **161**(7): p. 1681-96.
11. Waddell, N., et al., *Whole genomes redefine the mutational landscape of pancreatic cancer*. Nature, 2015. **518**(7540): p. 495-501.
12. Totoki, Y., et al., *Trans-ancestry mutational landscape of hepatocellular carcinoma genomes*. Nat Genet, 2014. **46**(12): p. 1267-73.
13. *Comprehensive molecular characterization of gastric adenocarcinoma*. Nature, 2014. **513**(7517): p. 202-9.
14. *Comprehensive molecular profiling of lung adenocarcinoma*. Nature, 2014. **511**(7511): p. 543-50.
15. Chantrill, L.A., et al., *Precision Medicine for Advanced Pancreas Cancer: The Individualized Molecular Pancreatic Cancer Therapy (IMPaCT) Trial*. Clin Cancer Res, 2015. **21**(9): p. 2029-37.
16. Dulak, A.M., et al., *Exome and whole-genome sequencing of esophageal adenocarcinoma identifies recurrent driver events and mutational complexity*. Nat Genet, 2013. **45**(5): p. 478-86.
17. Weaver, J.M., et al., *Ordering of mutations in preinvasive disease stages of esophageal carcinogenesis*. Nat Genet, 2014. **46**(8): p. 837-43.
18. Nones, K., et al., *Genomic catastrophes frequently arise in esophageal adenocarcinoma and drive tumorigenesis*. Nat Commun, 2014. **5**: p. 5224.
19. Cancer Genome Atlas Research, N., et al., *The Cancer Genome Atlas Pan-Cancer analysis project*. Nat Genet, 2013. **45**(10): p. 1113-20.
20. Nones, K., et al., *Genomic catastrophes frequently arise in esophageal adenocarcinoma and drive tumorigenesis*. Nat Commun, 2014. **5**: p. 5224.

21. Paterson, A.L., et al., *Mobile element insertions are frequent in oesophageal adenocarcinomas and can mislead paired-end sequencing analysis*. BMC Genomics, 2015. **16**: p. 473.
22. Tubio, J.M., et al., *Mobile DNA in cancer. Extensive transduction of nonrepetitive DNA mediated by L1 retrotransposition in cancer genomes*. Science, 2014. **345**(6196): p. 1251343.
23. Mermel, C.H., et al., *GISTIC2.0 facilitates sensitive and confident localization of the targets of focal somatic copy-number alteration in human cancers*. Genome Biol, 2011. **12**(4): p. R41.
24. Lawrence, M.S., et al., *Mutational heterogeneity in cancer and the search for new cancer-associated genes*. Nature, 2013. **499**(7457): p. 214-8.
25. Nik-Zainal, S., et al., *The life history of 21 breast cancers*. Cell, 2012. **149**(5): p. 994-1007.
26. Paterson, A.L., et al., *Characterization of the timing and prevalence of receptor tyrosine kinase expression changes in oesophageal carcinogenesis*. Journal of Pathology, 2013. **230**(1): p. 118-28.
27. Van Cutsem, E., et al., *HER2 screening data from ToGA: targeting HER2 in gastric and gastroesophageal junction cancer*. Gastric Cancer, 2014.
28. <http://public.ukcrn.org.uk/search/>. UKCRN Trial Portfolio. 2015 [cited 2015 22/11/15]; Available from: <http://public.ukcrn.org.uk/search/>.
29. Alexandrov, L.B., et al., *Signatures of mutational processes in human cancer*. Nature, 2013. **500**(7463): p. 415-21.
30. Shiraishi, Y., et al., *A Simple Model-Based Approach to Inferring and Visualizing Cancer Mutation Signatures*. PLoS Genet, 2015. **11**(12): p. e1005657.
31. Gehring, J.S., et al., *SomaticSignatures: inferring mutational signatures from single-nucleotide variants*. Bioinformatics, 2015. **31**(22): p. 3673-5.
32. Pearl, L.H., et al., *Therapeutic opportunities within the DNA damage response*. Nat Rev Cancer, 2015. **15**(3): p. 166-80.
33. Shen, J., et al., *ARID1A Deficiency Impairs the DNA Damage Checkpoint and Sensitizes Cells to PARP Inhibitors*. Cancer Discov, 2015. **5**(7): p. 752-67.
34. Hodi, F.S., et al., *Improved survival with ipilimumab in patients with metastatic melanoma*. N Engl J Med, 2010. **363**(8): p. 711-23.
35. Larkin, J., et al., *Combined Nivolumab and Ipilimumab or Monotherapy in Untreated Melanoma*. N Engl J Med, 2015. **373**(1): p. 23-34.
36. Herbst, R.S., et al., *Pembrolizumab versus docetaxel for previously treated, PD-L1-positive, advanced non-small-cell lung cancer (KEYNOTE-010): a randomised controlled trial*. Lancet, 2015.
37. Rizvi, N.A., et al., *Cancer immunology. Mutational landscape determines sensitivity to PD-1 blockade in non-small cell lung cancer*. Science, 2015. **348**(6230): p. 124-8.
38. Snyder, A., et al., *Genetic basis for clinical response to CTLA-4 blockade in melanoma*. N Engl J Med, 2014. **371**(23): p. 2189-99.
39. McGranahan, N., et al., *Clonal neoantigens elicit T cell immunoreactivity and sensitivity to immune checkpoint blockade*. Science, 2016. **351**(6280): p. 1463-9.
40. Van Allen, E.M., et al., *Genomic correlates of response to CTLA-4 blockade in metastatic melanoma*. Science, 2015. **350**(6257): p. 207-11.
41. Tumeh, P.C., et al., *PD-1 blockade induces responses by inhibiting adaptive immune resistance*. Nature, 2014. **515**(7528): p. 568-71.

42. Hamanishi, J., et al., *Programmed cell death 1 ligand 1 and tumor-infiltrating CD8+ T lymphocytes are prognostic factors of human ovarian cancer*. Proc Natl Acad Sci U S A, 2007. **104**(9): p. 3360-5.
43. Benafif, S. and M. Hall, *An update on PARP inhibitors for the treatment of cancer*. Onco Targets Ther, 2015. **8**: p. 519-28.
44. Oza, A.M., et al., *Olaparib combined with chemotherapy for recurrent platinum-sensitive ovarian cancer: a randomised phase 2 trial*. Lancet Oncol, 2015. **16**(1): p. 87-97.
45. Demel, H.R., et al., *Effects of topoisomerase inhibitors that induce DNA damage response on glucose metabolism and PI3K/Akt/mTOR signaling in multiple myeloma cells*. Am J Cancer Res, 2015. **5**(5): p. 1649-64.
46. Farmer, H., et al., *Targeting the DNA repair defect in BRCA mutant cells as a therapeutic strategy*. Nature, 2005. **434**(7035): p. 917-21.
47. Di Leonardo, A., et al., *DNA damage triggers a prolonged p53-dependent G1 arrest and long-term induction of Cip1 in normal human fibroblasts*. Genes Dev, 1994. **8**(21): p. 2540-51.
48. Agarwal, M.L., et al., *A p53-dependent S-phase checkpoint helps to protect cells from DNA damage in response to starvation for pyrimidine nucleotides*. Proc Natl Acad Sci U S A, 1998. **95**(25): p. 14775-80.
49. Brooks, K., et al., *A potent Chk1 inhibitor is selectively cytotoxic in melanomas with high levels of replicative stress*. Oncogene, 2013. **32**(6): p. 788-96.
50. Vera, J., et al., *Chk1 and Wee1 control genotoxic-stress induced G2-M arrest in melanoma cells*. Cell Signal, 2015. **27**(5): p. 951-60.
51. Liu, Q., et al., *Chk1 is an essential kinase that is regulated by Atr and required for the G(2)/M DNA damage checkpoint*. Genes Dev, 2000. **14**(12): p. 1448-59.
52. Watanabe, N., M. Broome, and T. Hunter, *Regulation of the human WEE1Hu CDK tyrosine 15-kinase during the cell cycle*. EMBO J, 1995. **14**(9): p. 1878-91.
53. van de Wetering, M., et al., *Prospective derivation of a living organoid biobank of colorectal cancer patients*. Cell, 2015. **161**(4): p. 933-45.
54. Sato, T., et al., *Single Lgr5 stem cells build crypt-villus structures in vitro without a mesenchymal niche*. Nature, 2009. **459**(7244): p. 262-5.
55. Ciriello, G., et al., *Emerging landscape of oncogenic signatures across human cancers*. Nat Genet, 2013. **45**(10): p. 1127-33.
56. Osato, M., *Point mutations in the RUNX1/AML1 gene: another actor in RUNX leukemia*. Oncogene, 2004. **23**(24): p. 4284-96.
57. <https://clinicaltrials.gov/>. 2015 22/06/15]; US National Institutes of Health trial registry]. Available from: <https://clinicaltrials.gov/>.
58. Watkins, J.A., et al., *Genomic scars as biomarkers of homologous recombination deficiency and drug response in breast and ovarian cancers*. Breast Cancer Res, 2014. **16**(3): p. 211.
59. Alexandrov, L.B., et al., *A mutational signature in gastric cancer suggests therapeutic strategies*. Nat Commun, 2015. **6**: p. 8683.
60. Ledermann, J., et al., *Olaparib maintenance therapy in patients with platinum-sensitive relapsed serous ovarian cancer: a preplanned retrospective analysis of outcomes by BRCA status in a randomised phase 2 trial*. Lancet Oncol, 2014. **15**(8): p. 852-61.
61. Verhagen, C.V., et al., *Extent of radiosensitization by the PARP inhibitor olaparib depends on its dose, the radiation dose and the integrity of the homologous recombination pathway of tumor cells*. Radiother Oncol, 2015. **116**(3): p. 358-65.

62. Kelly RJ, T.E., Zahurak. M, Cornish. T, Cuka. N, Abdelfatah. E, Taube. JM, Yang. S, Duncan. M, Ahuja. N, Murphy. A, Anders. RA, *Adaptive immune resistance in gastro-esophageal cancer: Correlating tumoral/stromal PDL1 expression with CD8+ cell count.* J Clin Oncol 2015. **33**(suppl; abstr 4031)).
63. Nakamura, H., et al., *Genomic spectra of biliary tract cancer.* Nat Genet, 2015. **47**(9): p. 1003-10.
64. Bridges, K.A., et al., *MK-1775, a novel Wee1 kinase inhibitor, radiosensitizes p53-defective human tumor cells.* Clin Cancer Res, 2011. **17**(17): p. 5638-48.
65. Wang, Y., et al., *Radiosensitization of p53 mutant cells by PD0166285, a novel G(2) checkpoint abrogator.* Cancer Res, 2001. **61**(22): p. 8211-7.
66. Liu, D.S., et al., *APR-246 potently inhibits tumour growth and overcomes chemoresistance in preclinical models of oesophageal adenocarcinoma.* Gut, 2015. **64**(10): p. 1506-16.
67. Stewart, A., et al., *Titration of signalling output: insights into clinical combinations of MEK and AKT inhibitors.* Annals of Oncology, 2015. **26**(7): p. 1504-10.
68. Li, H. and R. Durbin, *Fast and accurate short read alignment with Burrows-Wheeler transform.* Bioinformatics, 2009. **25**(14): p. 1754-60.
69. Saunders, C.T., et al., *Strelka: accurate somatic small-variant calling from sequenced tumor-normal sample pairs.* Bioinformatics, 2012. **28**(14): p. 1811-7.
70. McLaren, W., et al., *Deriving the consequences of genomic variants with the Ensembl API and SNP Effect Predictor.* Bioinformatics, 2010. **26**(16): p. 2069-70.
71. Van Loo, P., et al., *Allele-specific copy number analysis of tumors.* Proc Natl Acad Sci U S A, 2010. **107**(39): p. 16910-5.
72. McKenna, A., et al., *The Genome Analysis Toolkit: a MapReduce framework for analyzing next-generation DNA sequencing data.* Genome Res, 2010. **20**(9): p. 1297-303.
73. Zack, T.I., et al., *Pan-cancer patterns of somatic copy number alteration.* Nat Genet, 2013. **45**(10): p. 1134-40.
74. Boeva, V., et al., *Control-FREEC: a tool for assessing copy number and allelic content using next-generation sequencing data.* Bioinformatics, 2012. **28**(3): p. 423-5.
75. Li, H. *Aligning sequence reads, clone sequences and assembly contigs with BWA-MEM.* 2013 [cited 2015; Version 2:[Available from: <http://arxiv.org/abs/1303.3997>].
76. Chen, X., et al., *Manta: rapid detection of structural variants and indels for germline and cancer sequencing applications.* Bioinformatics, 2016. **32**(8): p. 1220-2.
77. Schulte, I., et al., *Structural analysis of the genome of breast cancer cell line ZR-75-30 identifies twelve expressed fusion genes.* BMC Genomics, 2012. **13**: p. 719.
78. Le Tallec, B., et al., *Common fragile site profiling in epithelial and erythroid cells reveals that most recurrent cancer deletions lie in fragile sites hosting large genes.* Cell Rep, 2013. **4**(3): p. 420-8.
79. Mir, A.A., C. Philippe, and G. Cristofari, *euL1db: the European database of L1HS retrotransposon insertions in humans.* Nucleic Acids Res, 2015. **43**(Database issue): p. D43-7.
80. Auton, A., et al., *A global reference for human genetic variation.* Nature, 2015. **526**(7571): p. 68-74.
81. Wilkerson, M.D. and D.N. Hayes, *ConsensusClusterPlus: a class discovery tool with confidence assessments and item tracking.* Bioinformatics, 2010. **26**(12): p. 1572-3.

82. Nilsen, G., et al., *Copynumber: Efficient algorithms for single- and multi-track copy number segmentation*. BMC Genomics, 2012. **13**: p. 591.
83. Korbel, J.O. and P.J. Campbell, *Criteria for inference of chromothripsis in cancer genomes*. Cell, 2013. **152**(6): p. 1226-36.
84. Puente, X.S., et al., *Non-coding recurrent mutations in chronic lymphocytic leukaemia*. Nature, 2015. **526**(7574): p. 519-24.
85. Kumar, P., S. Henikoff, and P.C. Ng, *Predicting the effects of coding non-synonymous variants on protein function using the SIFT algorithm*. Nat Protoc, 2009. **4**(7): p. 1073-81.
86. Adzhubei, I.A., et al., *A method and server for predicting damaging missense mutations*. Nat Methods, 2010. **7**(4): p. 248-9.
87. Lundegaard, C., et al., *NetMHC-3.0: accurate web accessible predictions of human, mouse and monkey MHC class I affinities for peptides of length 8-11*. Nucleic Acids Res, 2008. **36**(Web Server issue): p. W509-12.
88. Adiconis, X., et al., *Comparative analysis of RNA sequencing methods for degraded or low-input samples*. Nat Methods, 2013. **10**(7): p. 623-9.

‡oesophageal Cancer Clinical and Molecular Stratification (OCCAMS) Consortium:

Ayesha Noorani¹, Rachael Fels Elliott¹, Laura Smith¹, Zarah Abdullahi¹, Rachel de la Rue¹, Alison Cluroe², Shalini Malhotra², Richard Hardwick⁵, Mike L Smith⁴, Jim Davies⁶, Richard Turkington⁸, Stephen J. Hayes^{9,15}, Yeng Ang^{9,10,31}, Shaun R. Preston¹¹, Sarah Oakes¹¹, Izhar Bagwan¹¹, Vicki Save¹², Richard J.E. Skipworth¹², Ted R. Hupp¹², J. Robert O'Neill^{12,24}, Olga Tucker^{13,30}, Philippe Tanriere¹³, Fergus Noble¹⁴, Jack Owsley¹⁴, Laurence Lovat³, Rehan Haidry³, Victor Eneh³, Charles Crichton¹⁶, Hugh Barr¹⁷, Neil Shepherd¹⁷, Oliver Old¹⁷, Jesper Lagergren^{18,25,26}, James Gossage^{18,25}, Andrew Davies^{18,25}, Fujun Chang^{18,25}, Janine Zylstra^{18,25}, Grant Sanders¹⁹, Richard Berrisford¹⁹, Catherine Harden¹⁹, David Bunting¹⁹, Mike Lewis²⁰, Ed Cheong²⁰, Bhaskar Kumar²⁰, Simon L Parsons²¹, Irshad Soomro²¹, Philip Kaye²¹, Pamela Collier²¹, Laszlo Igali²², Ian Welch²³, Michael Scott²³, Shamila Sothi²⁷, Sari Suortamo²⁷, Suzy Lishman²⁸, Duncan Beardsmore²⁹, Hayley E. Francies³², Mathew J. Garnett³², John V. Pearson^{33,34}, Katia Nones^{33,34}, Ann-Marie Patch^{33,34}, Sean M. Grimmond^{34,35}

¹MRC Cancer Unit, University of Cambridge, Cambridge, UK

²Department of Histopathology, Addenbrooke's Hospital, Cambridge, UK

³University College London, London, UK

⁴Cancer Research UK Cambridge Institute, University of Cambridge, Cambridge, UK

⁵Oesophago-Gastric Unit, Addenbrooke's Hospital, Cambridge, UK

⁶Oxford ComLab, University of Oxford, UK

⁷Cambridge University Hospitals NHS Foundation Trust, Cambridge, UK

⁸Centre for Cancer Research and Cell Biology, Queen's University Belfast, Northern Ireland, UK

⁹Salford Royal NHS Foundation Trust, Salford, UK

¹⁰Wigan and Leigh NHS Foundation Trust, Wigan, Manchester, UK

¹¹Royal Surrey County Hospital NHS Foundation Trust, Guildford, UK

¹²Edinburgh Royal Infirmary, Edinburgh, UK

¹³University Hospitals Birmingham NHS Foundation Trust, Birmingham, UK

¹⁴University Hospital Southampton NHS Foundation Trust, Southampton, UK

¹⁵Faculty of Medical and Human Sciences, University of Manchester, UK

¹⁶Department of Computer Science, University of Oxford, UK

¹⁷Gloucester Royal Hospital, Gloucester, UK

¹⁸St Thomas's Hospital, London, UK

¹⁹Plymouth Hospitals NHS Trust, Plymouth, UK

²⁰Norfolk and Norwich University Hospital NHS Foundation Trust, Norwich, UK

²¹Nottingham University Hospitals NHS Trust, Nottingham, UK

²²Norfolk and Waveney Cellular Pathology Network, Norwich, UK

²³Wythenshawe Hospital, Manchester, UK

²⁴Edinburgh University, Edinburgh, UK

²⁵King's College London, London, UK

²⁶Karolinska Institutet, Stockholm, Sweden

²⁷University Hospitals Coventry and Warwickshire NHS, Trust, Coventry, UK

²⁸Peterborough Hospitals NHS Trust, Peterborough City Hospital, Peterborough, UK

²⁹Royal Stoke University Hospital, UHNM NHS Trust, UK

³⁰Institute of cancer and genomic sciences, University of Birmingham

³¹GI science centre, University of Manchester, UK

³²Wellcome Trust Sanger Institute, Wellcome Trust Genome Campus, Hinxton, UK

³³Department of Genetics and Computational Biology, QIMR Berghofer, Herston, Queensland, Australia

³⁴Queensland Centre for Medical Genomics, Institute for Molecular Bioscience, The University of Queensland, Queensland, Australia

³⁵Victorian Comprehensive Cancer Centre, University of Melbourne, Melbourne, Australia

Table 1. *In vitro* cytotoxicity of RTKi as single or combined reagents in EAC cell lines. Key RTK amplification status and drug targets are shown. Highlighting indicates that a synergic effect of the combination treatment was observed.

Cell line	RTK status	RTKi	GI50 (95% CI) (nM)	AUC
OE33	ERBB2/MET Amp	Lapatinib (EGFR/ERBB2)	3.92 x103 (3.16-4.87 x103)	195.7
		Crizotinib (MET)	317.3 (166.3-605.4)	108.8
		Lapatinib + Crizotinib	6.56 (2.42-17.84)	47
SK-GT-4	ERBB2 Amp/MET Gain	Lapatinib (EGFR/ERBB2)	3.72 x103 (2.27-6.08 x103)	173.9
		Crizotinib (MET)	3.47 x103 (2.90-4.15 x103)	183.2
		Lapatinib + Crizotinib	530 (273.1-1029)	120
OAC-P4C	ERBB2/FGFR2 Amp	Lapatinib (EGFR/ERBB2)	2.28 x103 (1.34-3.90 x103)	159.1
		AZD-4547(FGFR1/2/3)	3.82 x103 (3.32-4.40 x103)	194.7
		Lapatinib + AZD-4547	373.2 (260.9-533.7)	104.8
Flo	EGFR/MET Gain	Lapatinib (EGFR/ERBB2)	11.64 x103 (7.80-17.39 x103)	212
		Crizotinib (MET)	1.90 x103 (1.51-2.39 x103)	159.3
		Lapatinib + Crizotinib	243.4 (78.0-759.5)	109
OES127	ERBB2 Amp/MET Gain	Lapatinib (EGFR/ERBB2)	1.14 x103 (0.68-1.90 x103)	139.6
		Crizotinib (MET)	3.09 x103 (2.35-4.05 x103)	173.4
		Lapatinib + Crizotinib	587.7 (450.5-766.7)	117.5

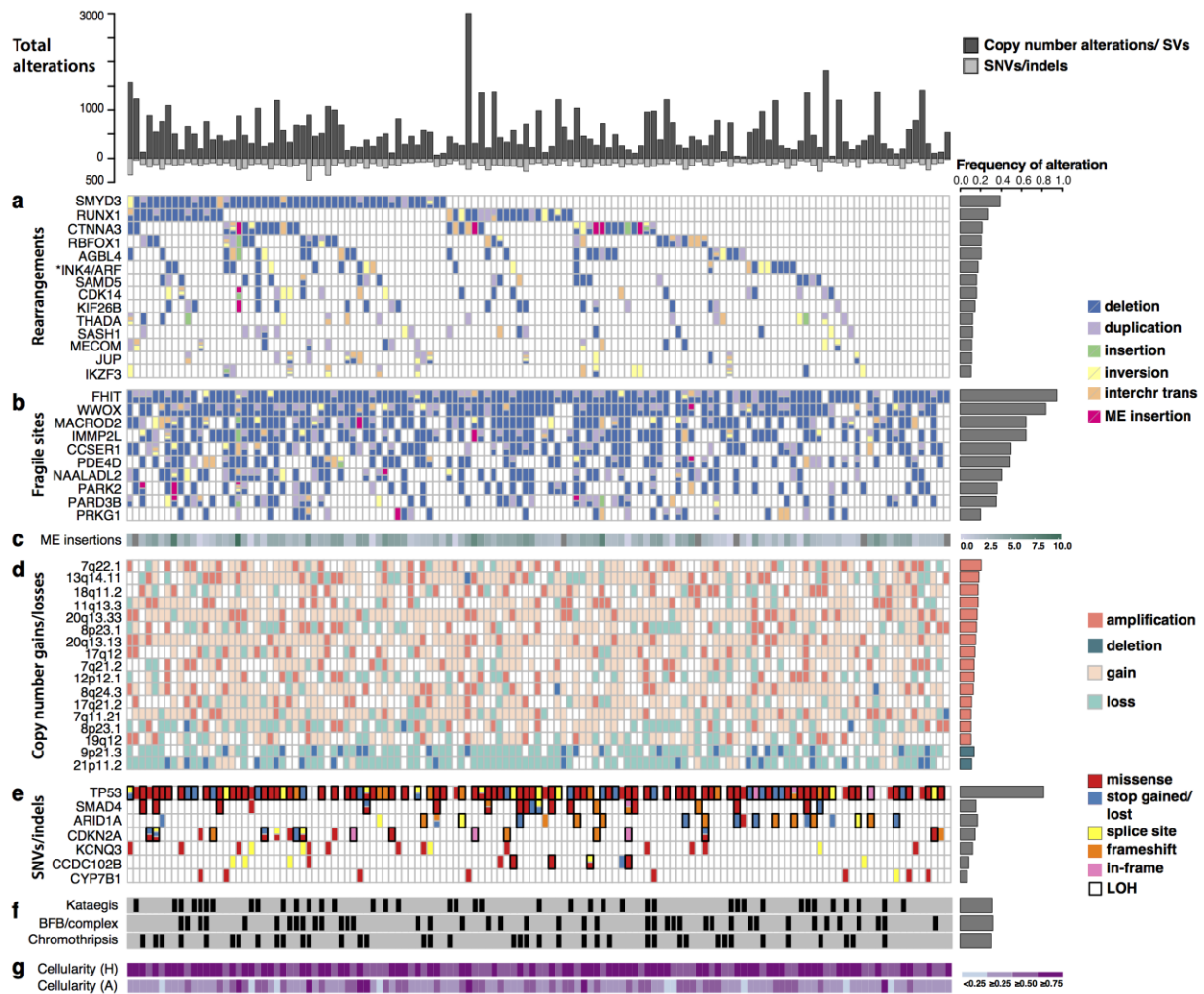


Figure 1. Recurrent genomic events in the cohort (n=129). The top panel highlights the total number of protein-coding genes affected by copy number or structural changes (above the 0 axis), and point mutations or indels (below the 0 axis), respectively, for every patient (depicted on the X-axis). (a) The top rearranged genes, excluding fragile sites, containing structural variant hotspots and recurrent in >10% of patients. *INK4/ARF comprises the CDKN2A/2B locus. (b) Fragile sites rearranged in at least 20% of the patients. (c) Mobile element (ME) insertions detected by structural variant analysis, plotted on a log₂ scale. Grey tiles correspond to cases without any evidence of ME insertions. (d) Loci that are significantly amplified/deleted according to GISTIC2.0 and that are recurrent in >10% of the patients. The most extreme copy number alteration within the locus is shown for each patient (see Supplementary Tables 2 and 3 for lists of genes in such loci). Only amplification and deletions are counted for the frequency histogram. (e) Genes altered by nonsynonymous SNVs/indels, deemed significantly mutated by MutSigCV. Loss of heterozygosity (LOH) regions are indicated in black rectangles when the gene also presents a mutation, indicating likely loss of function. (f) Presence of genomic catastrophes. (g) Cellularities, estimated by histopathology (H) or computationally using ASCAT (A). All samples sequenced have passed the histopathological cellularity cut-off of 70%. The total frequency of a specific gene alteration or event in the cohort is shown on the right-hand side for each panel.

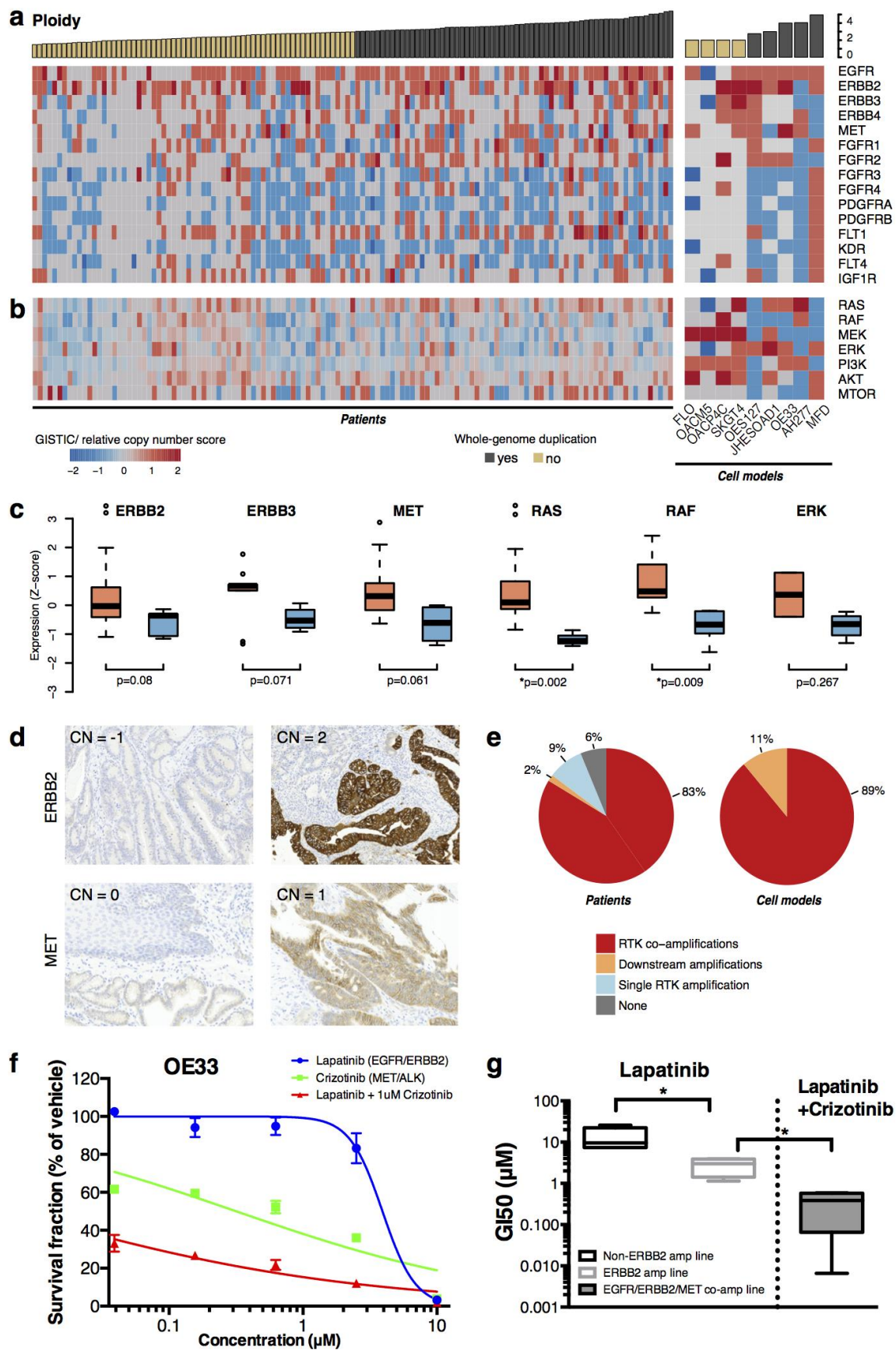


Figure 2. RTK copy number profiling and responses to targeted RTK therapy (n=129). (a) RTK copy number gains/losses in the cohort of patient-derived samples and 9 cell models. The copy number scores

refer to: amplifications (2), homozygous deletions (-2), relative gains/losses (+1/-1) (Methods). Columns correspond to samples, ordered by the average ploidy. Samples with average ploidy ≥ 3 are highlighted as potentially whole-genome duplicated. (b) Copy number alterations in key genes of downstream pathways (c) Expression of RTKs and downstream key genes in patient-derived samples with gains (light red) versus losses (light blue) of the respective genes. An asterix (*) marks p-values <0.05 after multiple testing correction. (d) IHC staining of selected samples displaying consequences of copy number loss/gain in ERBB2 and MET. The GISTIC score (CN) is marked in every case. (e) Breakdown of major resistance mechanisms to RTK-based monotherapy within the patient-derived sample cohort and the cell line cohort. "Amplified" for this analysis denotes anything with a score ≥ 1 . (f) Growth curve of OE33 cell lines after 72-hour exposure to Lapatinib, Crizotinib and in combination. Mean values as a percentage of DMSO treated cells and \pm SD for three experiments are shown. Olaparib used in combination was kept at $1\mu\text{M}$. (g) The effects of Lapatinib, Crizotinib and in combination on the cell lines with varying RTK status. Cell lines were grouped by the status of its relative RTK copy number into non-, ERBB2 amplification, and ERBB2 (or EGFR)/MET co-amplification. Error bars represent the standard deviation. An asterix(*) indicates p-values <0.05 .

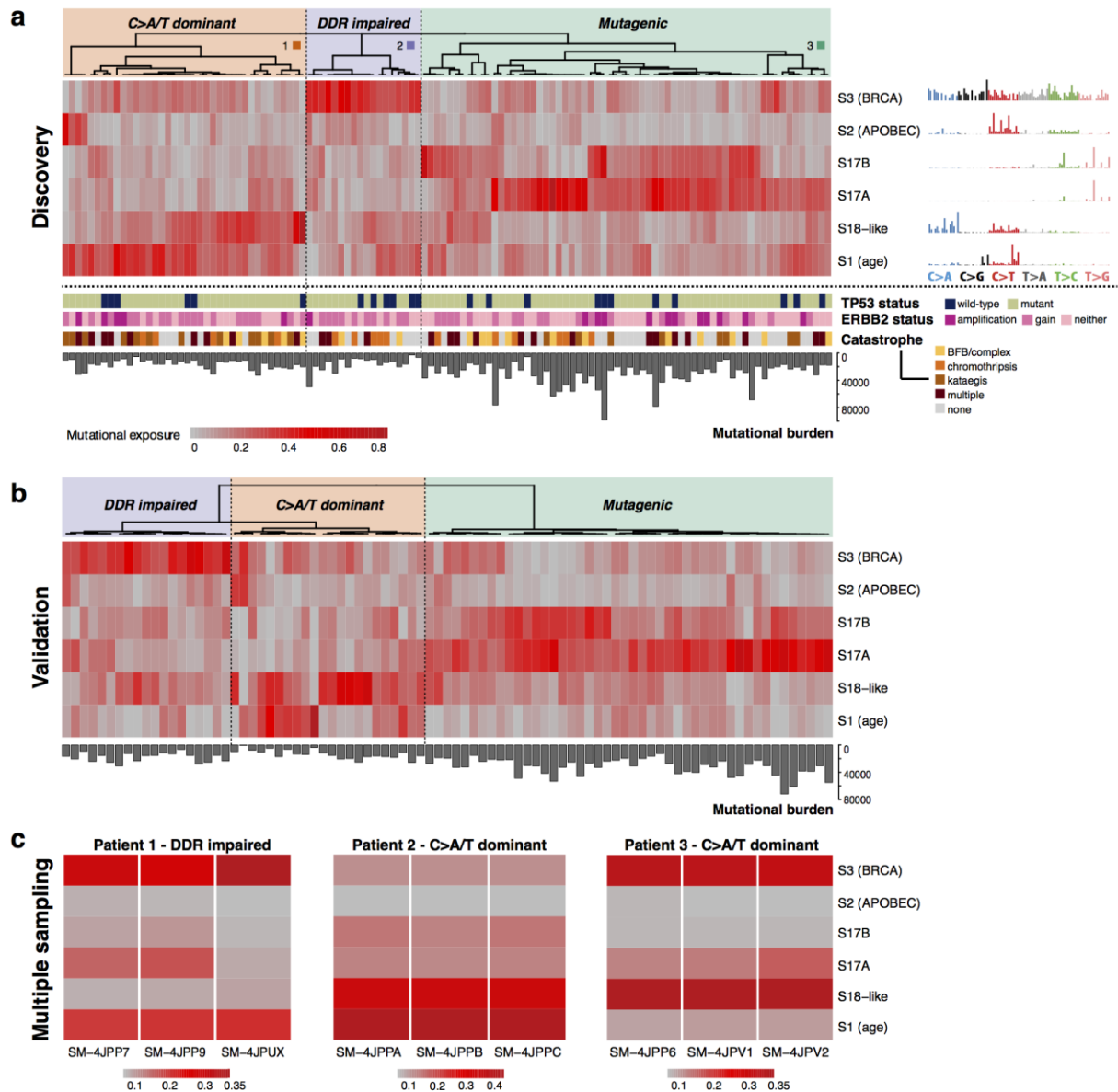


Figure 3. Mutational signature-based clustering reveals differences in disease etiology in the cohort and is spatially consistent within a single tumor. (a) The heat map highlights the sample exposures to six main mutational signatures, as identified in the cohort (n=120) using the NMF methodology. The strength of exposure to a certain signature may vary from 0% to 100% (on a color scale from grey to red). Three main subgroups can be observed from the clustering based on the predominant signature: C>A/T dominant (S18-like/age) – 38 samples, DDR impaired (BRCA) – 18 samples, and mutagenic (S17) – 64 samples. The TP53, HER2 status, and catastrophic event distribution in the corresponding genomes are highlighted below (no significant difference observed among subgroups). The total mutational burden is significantly higher in the mutagenic subgroup. Consensus clustering was used for the heat map (Methods). (b) Validation of the mutational signature-based clustering in an independent cohort (n=87). Unsupervised hierarchical clustering (Pearson correlation distance, Ward linkage method) reveals three main subgroups, similar to the ones in the discovery cohort: (1) S3 (BRCA) dominant – purple, 22% of the cohort; (2) mixed S18-like and S1 (age) – orange, 25% of the cohort; (3) S17A/B dominant – green, 53% of the cohort. The total SNV burden is also highlighted, confirming higher abundance in the mutagenic subgroup. (c) Mutational signature contributions in three cases with multiple sampling from the same tumor. The relative exposures to the 6 signatures are highlighted on a grey-to-red gradient for each case. The group assignment is based on the dominant signature.

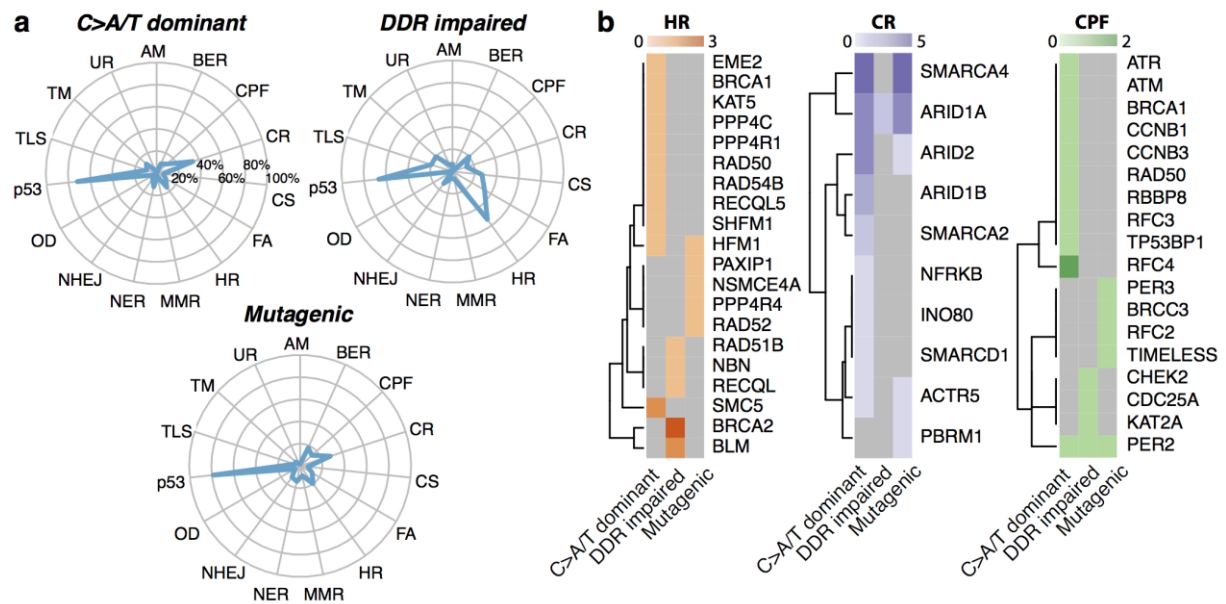


Figure 4. DNA damage repair pathways altered through nonsynonymous mutations/indels in the cohort. (a) For each of the three defined subgroups, the percentage of patients harboring defects in the different DDR-related pathways is shown. Only nonsynonymous mutations in genes mutated in the cohort significantly more compared to the expected background rate and predicted to be potentially damaging to the protein structure (Methods) have been considered in the analysis. (b) HR, CR and CPF genes altered in the three subgroups (the numbers in the gradients indicate how many patients have mutations in the respective gene). AM, alternative mechanism for telomere maintenance; BER, base excision repair; CPF, checkpoint factor; CR, chromatin remodelling; CS, chromosome segregation; DR, direct repair; FA, Fanconi anaemia pathway; HR, homologous recombination; MMR, mismatch repair; NER, nucleotide excision repair; NHEJ, non-homologous end joining; OD, other double-strand break repair; TLS, translesion synthesis; TM, telomere maintenance; UR, ubiquitylation response.

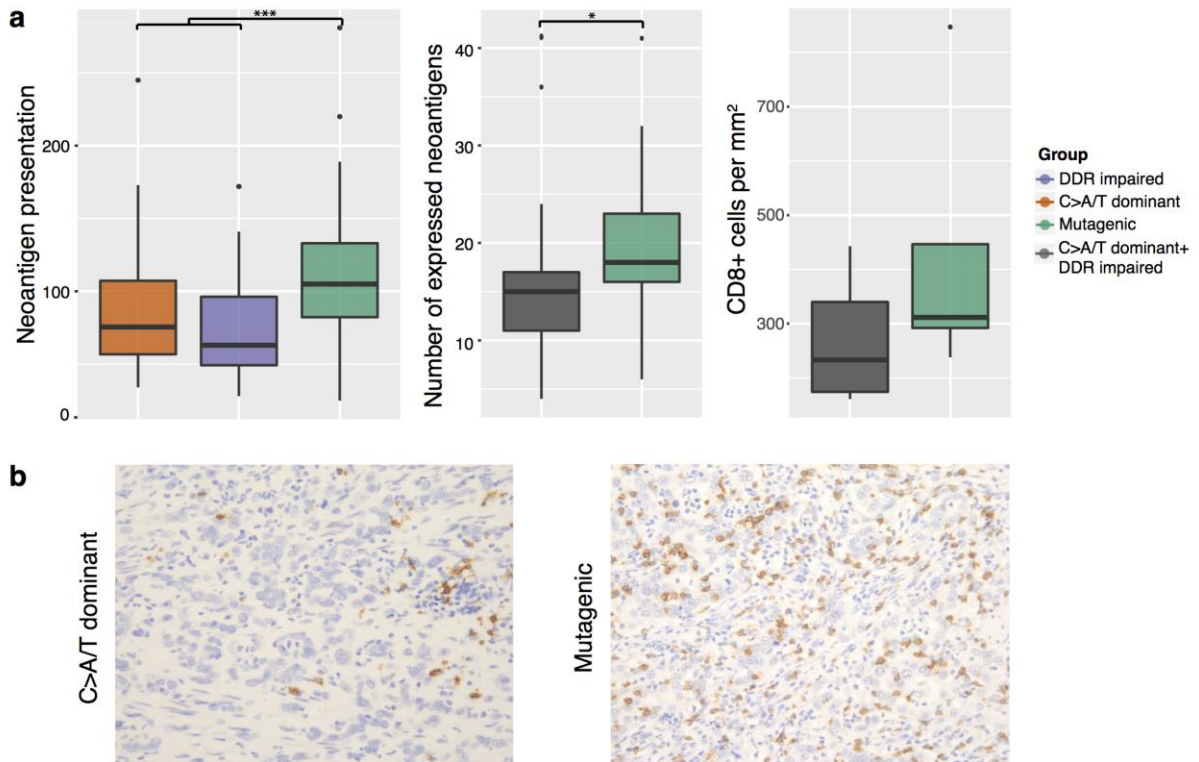


Figure 5. Neoantigen burden is significantly higher in the mutagenic subgroup and associates with an increased CD8+ T-cell density. (a) From left to right: (1) Neoantigen burden compared among the 3 mutational signature subgroups shows significant differences. A two-sided Welch's t-test was used to compare the mutagenic group to the rest; (2) Microarray and RNA-Seq data available for a subset of the samples (25 from the mutagenic subgroup and 21 from the others) reveals that the number of expressed potential neoantigens is significantly higher in the mutagenic subgroup (Wilcoxon rank-sum test $p = 0.042$); (3) Numbers of CD8+ T cells per mm² observed in patients. Patients were grouped into the mutagenic group and BRCA+C>A/T dominant group. (d) Two representative images of CD8 IHC staining from each group. Magnification: x200.

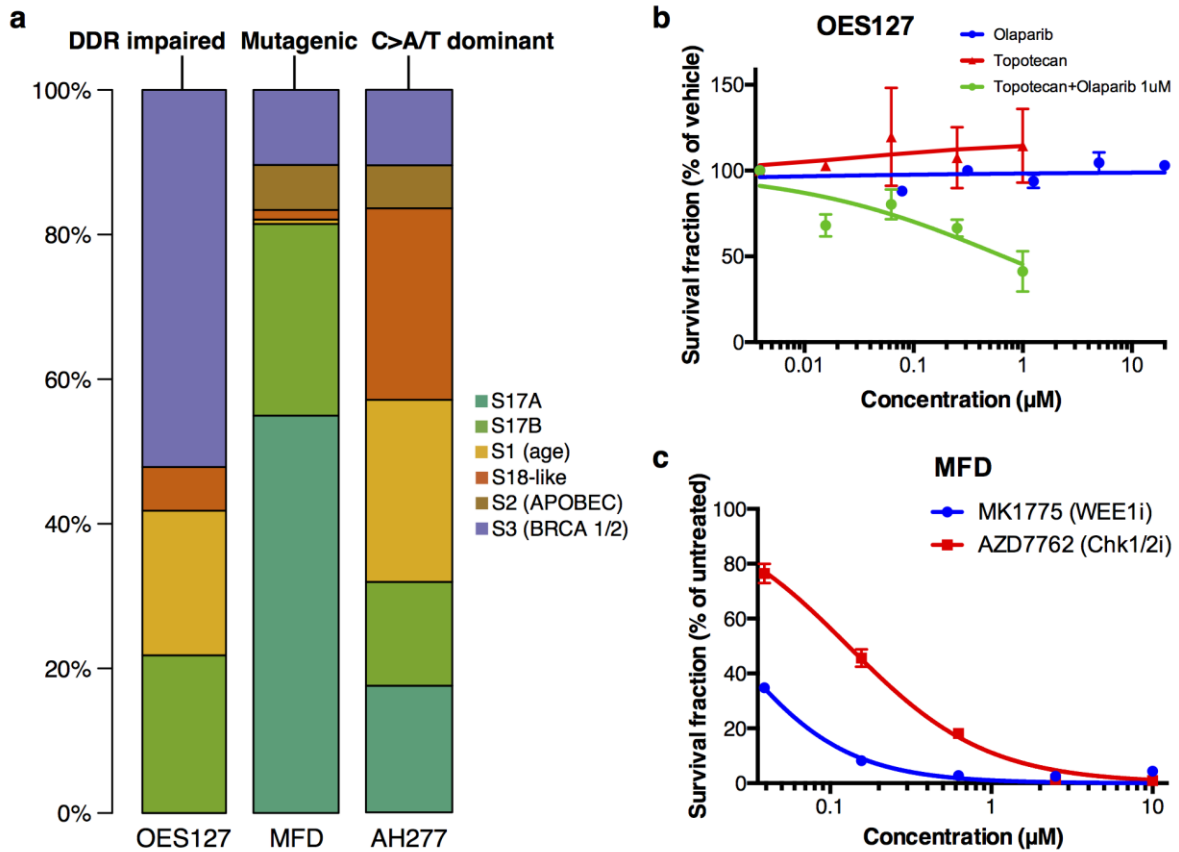


Figure 6. Treatment response in different mutational signature groups. (a) Three cell lines, OES127, MFD and AH277 have been derived, each representative of a distinct signature-dominant subgroup: DDR impaired (OES127), mutagenic (MFD) and C>A/T dominant (AH277). (b) Growth curves of OES127 cell lines after 72-hour exposure to Olaparib, Topotecan and in combination. Mean values as a percentage of DMSO treated cells and \pm SD for three experiments are shown. Olaparib used in combination was kept at 1 μM . (c) Growth curve of MFD cell lines after 72-hour exposure to MK-1775 and in AZD-7762. Mean values as a percentage of DMSO treated cells and \pm SD for three experiments are shown.

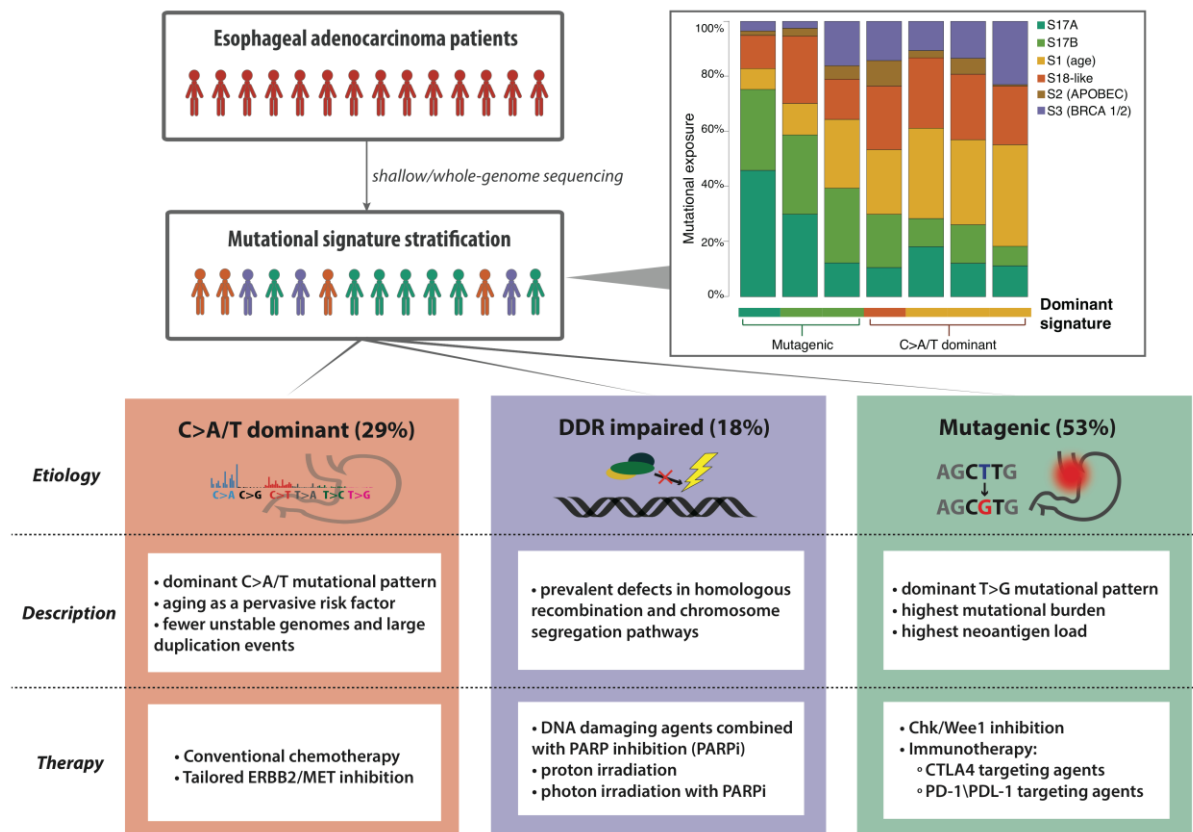


Figure 7. Proposed subclassification of EAC based on mutational signatures informs etiology and, consequently, potential tailored therapies to be further investigated for the disease. Patients are currently treated uniformly, but classification based on mutational signatures may enable targeted treatments that would complement classical therapy routes and potentially achieve more durable responses. The highlighted box (right) exemplifies classifying new patients into the defined etiological categories based on mutational signatures using a quadratic programming approach (see Methods). The bars highlight the relative contributions of the six expected signatures to the observed mutations in 7 new tumors (not part of the 129 sample cohort). The dominant signature is indicative of the group to which the sample should be assigned.